ORIGINAL PAPER

A highly uniform lamination micromixer with wedge shaped inlet channels for time resolved infrared spectroscopy

**Wolfgang Buchegger · Christoph Wagner ·
Bernhard Lendl · Martin Kraft · Michael J. Vellekoop**

Abstract We present a horizontal multi-lamination micromixer with specially wedge shaped vertical fluid inlets for fast and highly uniform fluid mixing in the low millisecond range. The four-layer laminar flow is created by a fluidic distribution network, reducing the amount of fluid connectors to the macroscopic world to two. All the geometries of the channel inlets and the distribution network were optimized for low flow rates and hence for low sample consumption using CFD simulations. The device materials applied feature low absorption in the mid-infrared (wavelength 3–10 μm) allowing to use this device for time resolved infrared spectroscopy. The micromixer itself can be built by silicon micromachining techniques without the need of complicated fabrication steps. Due to a transparent calcium fluoride cover optical measurements are possible as well which were used to characterize the device. Mixing times in the range of 1 ms with optical color measurements of aqueous solutions and with time resolved infrared measurement of the proton exchange reaction of H_2O and D_2O are achieved.

W. Buchegger (✉) · M. J. Vellekoop
Institute of Sensor and Actuator Systems,
Vienna University of Technology, Vienna, Austria
e-mail: wolfgang.buchegger@tuwien.ac.at

C. Wagner · B. Lendl
Institute of Chemical Technologies and Analytics,
Vienna University of Technology, Vienna, Austria

M. Kraft
Carinthian Tech Research AG, Villach, Austria

1 Introduction

Many advancements in the field of on-chip biological and biomedical analysis systems have been made in the last decades with the goal to decrease reagent consumption, lower processing time, increase throughput, lower the cost, introduce disposable platforms or to study new phenomena (Nguyen and Wereley 2002; Hardt et al. 2005). In biological or medical processes two or more reagents need to be mixed before a reaction can occur. The mixing must be fast and uniform at micrometer scale so that the reaction can fully develop and reaction dynamics can be studied.

In general, mixers can be divided into active and passive mixing principles. Active mixers need external energy or actuation and are, therefore, often more complex while passive mixers rely on diffusion or chaotic advection and are operated autonomously. A review summarizing the most common design approaches is given by Nguyen and Wu (2005), Mansur et al. (2008). A simple electromagnetically actuated micromixer was presented by Wen et al. (2009) with mixing times in the 1 s range. Designs utilizing acoustic waves achieved mixing times down to 7 ms (Ahmed et al. 2009; Johansson et al. 2009). Another active mixing principle with an actuated cantilever in the mixing channel was investigated by Williams et al. (2009) without stating actual mixing times. Mao et al. (2010) presented a chaotic bubble mixer with mixing times of 20 ms which uses monodisperse microbubbles for stirring. To overcome the need of an external energy source, which often leads to a complex device design, passive mixing principles are attractive. The probably most investigated passive mixing

principle is based on a T-shaped channel crossing, a so called T-mixer, with several channel variations. Mixing times in the 1 s range can be achieved with these designs in low Reynolds number flow regimes (Hossain et al. 2009). To reduce mixing time in T-mixers in the order of one magnitude, pillar structures (Chen et al. 2009) or herringbone structured walls (Park et al. 2010; Cortes-Quiroz et al. 2009) can be used, which introduce chaotic advection of the fluid. As many chemical and biochemical reaction times occur in the millisecond range, fast mixing at low flow rates, and thus small sample consumption, is desirable. Because the infrared (IR) absorption of aqueous solutions can be dominant compared to IR absorption changes caused by chemical reactions, the mixing channel height should not exceed 8–10 μm and be constant along the measurement section. The reduced cross section area of the mixing channel combined with a low flow rate, results in very low Reynolds numbers ($Re < 1$). This indicates strictly laminar flow conditions and mixing only occurs due to diffusion. Gambin et al. (2010) presented a design recently, which uses three dimensional flow focusing for fast mixing. However, this design with a focusing spot of about 5 μm is not applicable for IR spectroscopy because a measuring spot of about 150 μm in diameter is necessary to gain an acceptable signal to noise ratio. High aspect ratio laminar flow sheets were firstly used by Hinsmann et al. (2001a) for a stopped flow mixing device. The mixing time t of a diffusion based mixing system scales inversely proportional with the diffusion coefficient D and direct proportional with the square of the diffusion length d_{diff}:

$$t \propto \frac{d_{\text{diff}}^2}{D}. \tag{1}$$

A multilaminar flow design was presented by Kauffmann et al. (2001) and a similar design by Lipman et al. (2003) with mixing times of 50 ms. Figure 1a shows a laminar fluid structure with two layers (left) and four layers (right). In the right image the layers in the middle differ in thickness compared to the layers next to the channel wall. According to Eq. 1, the mixing time can be reduced by a factor of nine with this approach. A first design utilizing layers that differ in thickness was introduced by Kanai et al. (2002). Simulations show that with diffusion lengths of around 1 μm, mixing times of 1 ms are possible assuming fluid properties of water. However, if a multilaminar flow structure is used the off-chip effort increases as for every layer a fluid pump is needed or complicated fabrication steps are necessary to cross over fluid channels.

2 Materials and methods

In our design presented here, different fluid layers were laminated in a horizontal way by four vertical channels
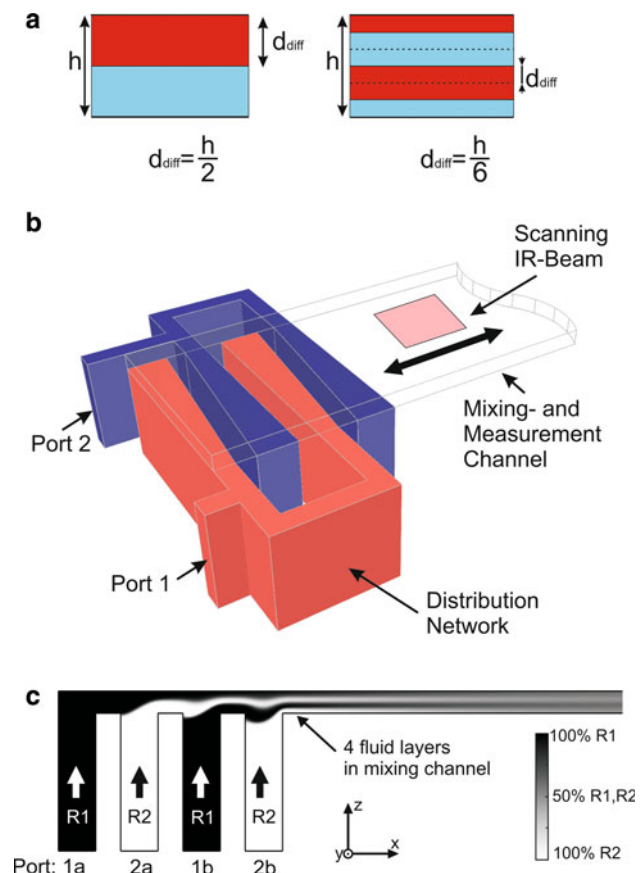

Fig. 1 a Cross section of fluidic channel with two lamination layers left and four lamination layers right. By doubling the layers from two to four the diffusion length decreases by a factor of three, the diffusion time by a factor of nine. **b** Schematic of the micromixer, forming four lamination layers. Two different reagents are pumped into ports 1 and 2. The mixing channel itself serves as measurement area. By moving the scanning IR-beam along the channel a time resolved measurement is achieved. **c** Two dimensional flow simulation of the micromixer to determine the individual flow velocities of each channel inlet for optimizing the thickness of each fluid layer

which lead into a horizontal mixing channel. A schematic of the design is given in Fig. 1b which shows the filled fluid channels, the wedge shaped inlet channels, and the mixing channel (Rigler et al. 2008). In order to keep the fluidic setup as simple as possible, the inlet channels with the same reagent are fed from one side through a fluidic distribution network. The exterior fluid connectors are indicated by ports 1 and 2 for the two different reagents. In contrary to previously presented designs, this system can be supplied by one double-syringe pump. To achieve the shortest mixing time and low premixing, the number of lamination layers in combination with the channel dimensions and geometry were investigated by computational fluid dynamics (CFD) simulations with *Comsol Multiphysics*. Simulations showed that wedge shaped inlets yield much faster mixing than straight inlets. The difference in

mixing performance between this novel wedge design and the classical straight design is investigated with simulations and measurements in the following.

2.1 Simulations

In first simulations the feeding channels and the fluid distribution network were designed before a full three dimensional model was investigated. For fully simultaneous diffusion of all lamination layers their thickness was varied until unwanted effects like premixing were minimized. Different flow velocities of the fluid junctions are also comprised in the simulations. To generate an individual optimum for each layer thickness, a fluid distribution network utilizes the pressure drop along a microchannel to feed the inlet channels with different fluid velocities. These velocities were predetermined by a two dimensional simulation of the micromixer shown in Fig. 1c. In this simulation port 1 was modeled with a reagent concentration R1 of 1 mol/m^3 and port 2 with a reagent concentration R2 of 0 mol/m^3. The diffusion coefficient was set to $D = 5 \cdot 10^{-10}$ m^2/s to suppress mixing and clearly show the different fluid layers. In addition, a flow rate of 30 μl/min was chosen, which is the maximum flow rate used with this micromixer. The resulting values of the relative flow velocities in the inlet channels are given in Table 1. These were used to design the fluidic distribution network according to Eq. 2 which gives the pressure drop ($\frac{dp}{dx}$) depending on the change in flow rate $\dot{Q}$ in rectangular channels (b = channel width, h = channel height and $h < b$), where η means the dynamic viscosity (Nguyen and Wereley 2002).

$$\dot{Q} = \frac{4bh^3}{3\eta}\left(-\frac{dp}{dx}\right)\left[1 - \frac{192b}{\pi^5 h}\sum_{i=1,2,3...}^{\infty}\frac{\tanh\left(\frac{i\pi h}{2b}\right)}{i^5}\right] \quad (2)$$

The cross section of the concentration profile of a three dimensional micromixer design is shown in Fig. 2. The channel width was set to $b = 200$ μm so if the measurement spot of the IR-spectrometer is placed in the middle there will be an edge of 25 μm on each side. These areas are excluded from the measurement to cancel time differences occurring at the border fluid layers due to the parabolic velocity profile caused by the pressure driven flow. To gain a lower off-chip complexity, each inlet is fed from

one side. A certain pressure drop occurs between the injecting and the far side of the channel inlet. This causes an inhomogeneous velocity and pressure distribution and hence non-uniform layers of fluid, as depicted in Fig. 2, profile A. Therefore, fast mixing of the reagents is inhibited. The cross sections in Fig. 2 show the four fluid layers in the mixing channel right after they are formed (profile A) and 50 μm after the layers were formed (profile B). The distance between profile A and B equals 2.5 ms with the used flow rates. Proper mixing is only occurring in the middle areas and the lamination structure in Fig. 2 profile A shows a kind of a zigzag shape. This limits the time resolution of the mixing chip because dynamic measurements can only be recorded of chemical reactions slower than the mixing procedure. To reduce the mixing time and form uniform fluid layers, the contact surface is increased by using a special geometry for the lamination inlets. The inlet broadens to a wedge shape at the far end of the feeding, resulting in a constant pressure distribution and hence uniform fluid layers.

An integration of the z-component of the fluid velocity over the channel width (y-component) gives information about the amount of fluid Q' added into the channel corresponding to Eq. 3
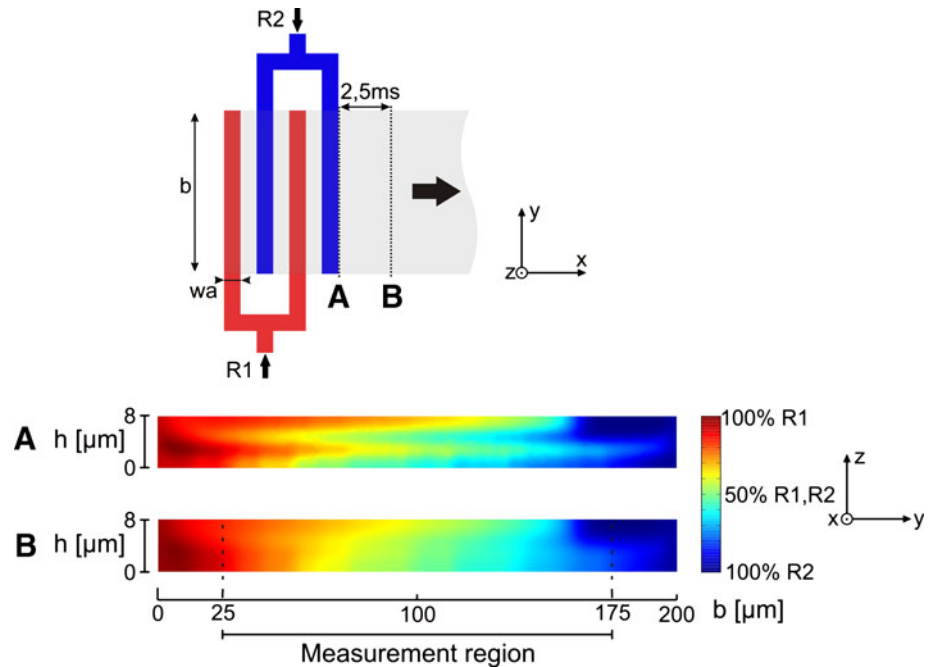
$$Q'(y) = \int v_z(x,y)dx. \quad (3)$$

The result of this integration is plotted on the y-axis, see Fig. 3a. In the two dimensional plot the x-axis shows the channel width b with the measurement region from 25 to 175 μm. If the quantity Q' is constant over the width of the mixing channel, uniform fluid layers are formed. The optimum geometry is found by comparing the variation of Q' in the measurement area:

$$\Delta Q = \int_{25\,\mu m}^{175\,\mu m} \frac{\left|Q'(y) - \overline{Q'(y)}\right|}{\overline{Q'(y)}}dy. \quad (4)$$

A graphical illustration of ΔQ is given in Fig. 3b. The best results can be achieved with a wedged inlet channel opening from $w_b = 10$ μm to $w_e = 22$ μm. As a result, the pressure and hence the flow velocity variations are below 3% of their mean value. The geometry of this optimized wedge shape is strongly depending on the depth of the feeding channel (200 μm in this design), the inlet channel width ($w_e = 10$ μm), the mixing channel height ($h = 8$ μm) and the flow velocity if varied in a wide range.

The simulation of Fig. 2 was repeated with the calculated wedge shape of $w_b = 10$ μm and $w_e = 22$ μm. A top view of the schematic and the corresponding concentration profile at the same times as in Fig. 2 are given in Fig. 4. In contrary to the straight shaped micromixer, profile A shows uniform lamination layers. Due to this precondition, the

Table 1 Simulation result of normalized flow rates for the optimal non-uniform lamination layers

Lamination inlet	Normalized flow rates
Port 1a	0.18
Port 1b	0.32
Port 2a	0.375
Port 2b	0.125

mixing performance in profile B yields far better results. The region of ±10% of ideal mixing concentration ranges over a total width of 160 μm in a channel of 200 μm width, which perfectly suits the IR measurement region of $150 \times 150\ \mu m^2$.

A simulation of the mixing performance at a flow rate of 30 μl/min and with four different diffusion coefficients is given in Fig. 5. The diffusion coefficients model different solutions, for instance, $D = 2 \cdot 10^{-9}\ m^2/s$ models the diffusion coefficient of aqueous solutions (Crowell and Bartels 1996) whereas $D = 5 \cdot 10^{-10}\ m^2/s$ models the diffusion of large biomolecules in aqueous solutions (e.g., proteins) which diffuse much slower. However, after a distance of $x_{90} = 200\ \mu m$ in the channel, a mixing quality of 90% is reached for a diffusion coefficient of $D = 2 \cdot 10^{-9}\ m^2/s$ which corresponds to a mixing time of $t_{90} = 0.64\ ms$.

2.2 Fabrication

The micromixer was fabricated according to the process depicted in Fig. 6 by silicon micromachining techniques on a silicon (Si) wafer (360 μm thick, double-side polished, silicon-nitride covered, ⟨100⟩ lattice orientation) and a calcium fluoride (CaF$_2$) wafer (1 mm thick, Korth Kristalle GmbH, Altenholz, GER). Both wafers have a diameter of 100 mm. The fluid inlets and the distribution network were processed on the silicon wafer. The photoresist AZ6612 and the resist developer AZ826 used for these steps were purchased from AZ Electronic Materials (Branchenburg, NJ, USA). The mixing channel was structured in WL-5150,

a photopatternable spin-on silicone (Dow Corning Corporation, Midland, MI, USA), on the CaF$_2$ wafer. To utilize this device for IR spectroscopy, it was necessary to use materials with low absorption in the mid IR region (3–10 μm). Silicon and calcium fluoride suit these requirements and CaF$_2$ is also transparent in the visible region so that this microchip can also be used for optical measurements with a light microscope. For more details about the IR absorption of materials and the setup of the IR spectrometer see Hinsmann et al (2001). Other cleanroom chemicals used for processing steps were alkali hydroxide etchant-KOH, propylene glycol monomethyl ether acetate-PGMEA and for cleansing ethanol, acetone, and isopropyl alcohol (Sigma Aldrich, St. Louis, MO, USA).

In the first step, the Si wafer was spin coated with a positive photoresist (Fig. 6a). A photomask was used to pattern the inlet holes for the fluid connections. Silicon nitride (Si$_3$N$_4$) was partly removed by plasma etching, acting as etch mask for wet-etching. The inlet holes were wet-etched using KOH to form pyramidal grooves (Fig. 6b). To form the fluidic distribution network, a deep reactive ion etching (DRIE) process was applied on the other side of the silicon wafer after the inlet distribution structure was patterned by photolithography (Fig. 6c). For this process step precise backside alignment with a double-side mask-aligner was necessary to join the KOH etched grooves with the DRIE trenches. The fabrication was then continued by spincoating a calcium fluoride wafer with WL-5150 (Fig. 6d). This layer was soft baked before patterning of the mixing channel by UV-exposure. After a post-exposure bake, the desired pattern was developed
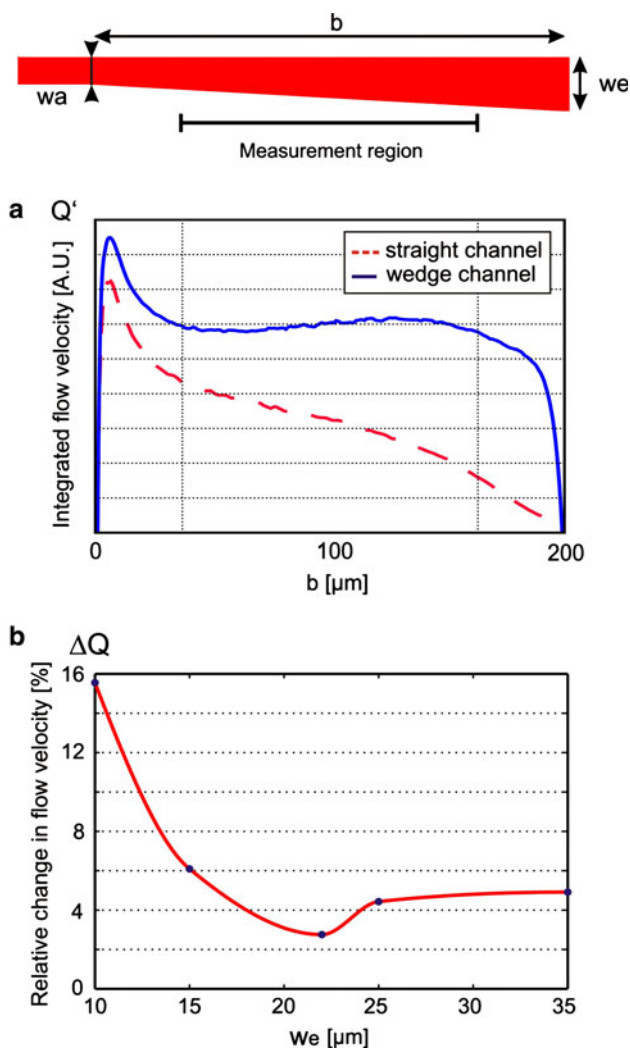
Fig. 3 a Integrated flow velocity Q' over the x-component of the inlet wedge. The homogeneity of Q' in the measurement area is crucial for uniform fluid layers. **b** The y-axis shows ΔQ, the relative change of the integrated flow velocity while the x-axis shows different values of w_e (w_a was fixed to 10 μm). The minimum of this plot defines the optimal wedge geometry for homogeneous fluid layers

(Fig. 6e). WL-5150 is an elastic material (bulk elongation 37.6 %) which allows bonding of silicon and calcium fluoride despite their highly different thermal expansion coefficients ($\alpha_{Si} = 2 \cdot 10^{-6} \, 1/K$ and $\alpha_{CaF_2} = 18.85 \cdot 10^{-6} \, 1/K$). The cold bonding procedure was applied for several hours at room temperature (Fig. 6f). The fully processed 100 mm wafer contains 40 devices (6×17 mm^2). To connect the microfluidic chip to a commercial syringe pump from KD Scientific Inc (Holliston, MA, USA), a custom holder was designed. To provide excellent chemical resistance combined with mechanical strength polyetheretherketon (PEEK), a partly crystalline plastic was chosen as material for the holder. The custom device holder with an integrated micromixer

is shown in Fig. 6. A window opening in the custom holder underneath the mixing channel enables measurements with a FTIR brightfield microscope.

2.3 Experimental results and discussion

2.3.1 Color experiment

A suitable reaction of two reagents was chosen to verify the simulation results. It is not possible to use a dyed and a colorless liquid to distinguish between a layered and a mixed system without a confocal microscope as the mixing principle relies on vertical diffusion and the mixing process is observed from top. As the mixing channel is only 8 μm high, a simple pH indicator was also not satisfactory because the color intensity was not sufficient. Therefore, we applied a very strong color reaction. Tests showed that the reaction of colorless thiocyanate (SCN$^-$) and slightly yellowish iron(III) (Fe^{3+}) solution forms a deep red complex of adequate color intensity (Fe^{3+} + SCN$^-$ → [FeSCN]$^{2+}$). For the following experiments 1.1 mol potassium thiocyanate KSCN and 0.1 mol iron(III) chloride FeCl$_3$ solutions were used. To get comparable results, the mixing quality M_Q was defined according to Eq. 5.

$$M_Q = \frac{I_m - I_{back}}{I_{cm} - I_{back}}. \tag{5}$$

To cancel the coloration intensity of the background image I_{back}, it is subtracted from the coloration intensities of the mixing experiment I_m and the completely mixed coloration value I_{cm}. In the experiment the micromixer was flushed solely with iron(III) solution and a premixed complex solution to get the respective color intensity values. For the experiment two micromixers, one with a wedge shaped inlet channel design and another one with a straight inlet channel design, was used. The mixers were driven by a dual syringe pump to gain stable and even flow rates ranging from 1 up to 30 μl/min in the mixing channel. Images were taken during the experiments with a digital camera applied to a microscope. The mixing times were calculated from the intensity values of a greyscale bitmap image by processing it with *Matlab* software.

The experimental result for the two different designs is shown in Figs. 7 and 8. An exponential curve fitting was applied for both measurements and the distance and time values at 90% mixing quality is calculated (x_{90} and t_{90}). In addition, a R-square value is given, showing the quality of the curve fitting, where one corresponds to a perfect fit. The resulting mixing time for the wedge shaped design of $t_{90w} = 0.9$ ms is in good agreement to the simulation results. The slightly faster result from the simulation could lead from a difference of the actual diffusion coefficient of

Fig. 4 Two dimensional concentration profile of the optimized wedge shaped micromixer at the point where the four fluid layers are formed and 2.5 ms further down the mixing channel. The reagents in channels 1 and 2 are dark colored. Proper mixing of the reagents is occurring in the bright region
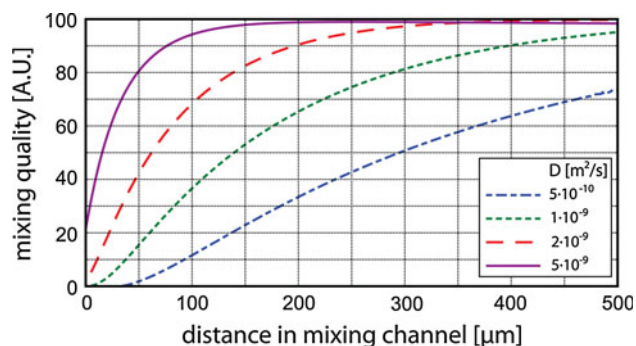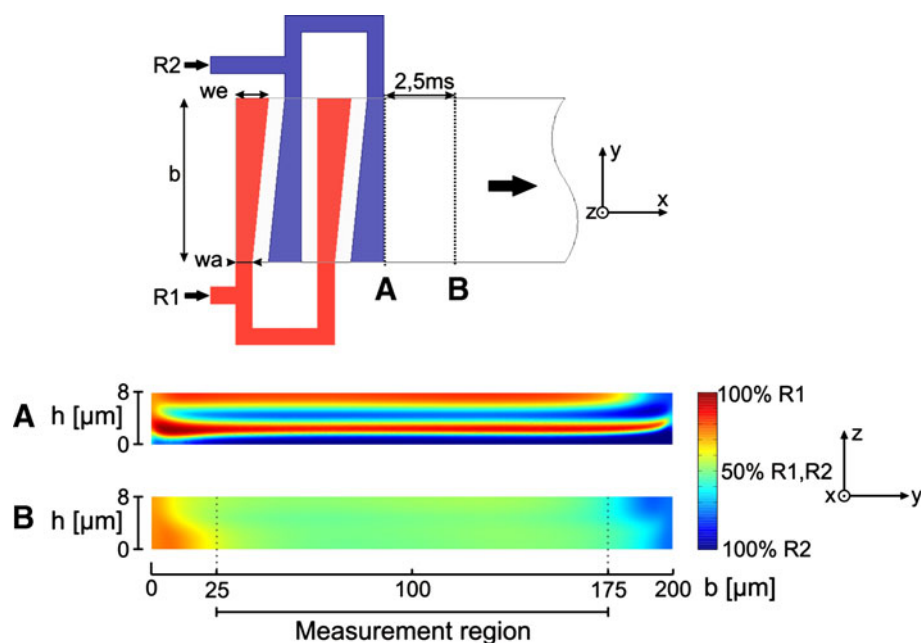

Fig. 5 Simulation result of the mixing performance with a flow rate of 30 μl/min in the mixing channel and different diffusion coefficients. The diffusion coefficient of $D = 2 \cdot 10^{-9}\,\mathrm{m^2/s}$ represents the diffusion of water molecules

the used reagents compared to the one used in the simulation model. A significant result is the improvement of mixing time of the wedge shaped design compared to the straight channel design in Fig. 8. The distance at which 90% mixing quality is reached for the straight channel design is not visible in Fig. 8, but was calculated from the exponential fit to be $x_{90s} = 1200\ \mu m$ This corresponds to a mixing time of $t_{90s} = 3.8$ ms which is a factor four slower compared to the optimized wedge design. Consequently, the wedge design leads to a higher time resolution when analyzing kinetics of fast chemical reactions (e.g., Jung et al. 2008).

2.3.2 IR experiment

This micromixer uses the mixing chamber of a diffusion mixer as measurement region for time resolved

measurements. Measuring close to the beginning of the mixing channel corresponds to shorter reaction times than when moving further down the channel in the flow direction. In the IR experiment the proton exchange reaction of H_2O and D_2O forming 2 HDO is investigated. This is a well-known reaction, which is commonly used for characterizing microfluidic devices used in IR spectroscopy (e.g.. Chan et al. 2009). Further, this reaction occurs between small water molecules which mix faster than larger biomolecules. If the measurement of the mixing procedure of such a fast reaction can be shown, it is obvious that other bioreactions, which are normally slower, can be measured with the device. The infrared measurements were carried out in transmission mode on a Hyperion 3000 microscope [Bruker Optics (Ettlingen, GER)], which was equipped with two 15-fold Cassegrain objectives. A mercury cadmium telluride (MCT) detector (Infrared Associates (Stuard, FL, USA)) with an element size of $250 \times 250\ \mu m^2$ was used. A picture of the optical beam path of the microscope is depicted in Fig. 1 ESM. The micromixing device was mounted in a custom chip holder and clamped onto the automated XY stage of the microscope. The two reagents were pumped through the mixer by a kdS 100 syringe pump (KD Scientific Inc (Holliston MA, USA)), which was equipped with two 500 μl syringes at a pumping speed of 15 μl/min per syringe resulting in a flow velocity of 31 cm/s in the mixing channel. The optical aperture of the microscope was limited to 150 μm width. The first measurement spot was positioned 75 μm downstream from the last outlet channel. By moving the mixer, placed on a XY stage, the measurement spots were equally spaced 150 μm apart. This resulted in a time resolution of
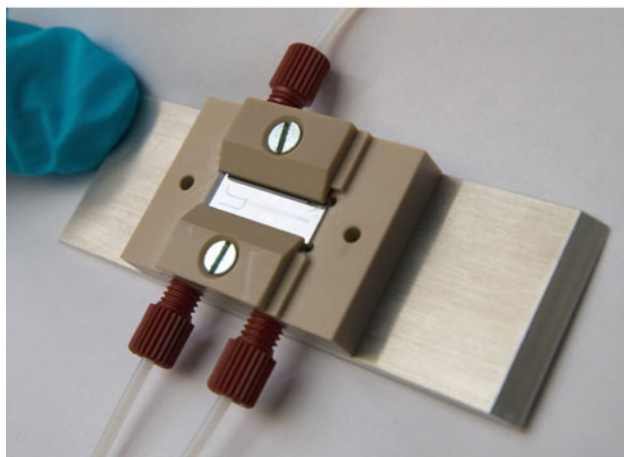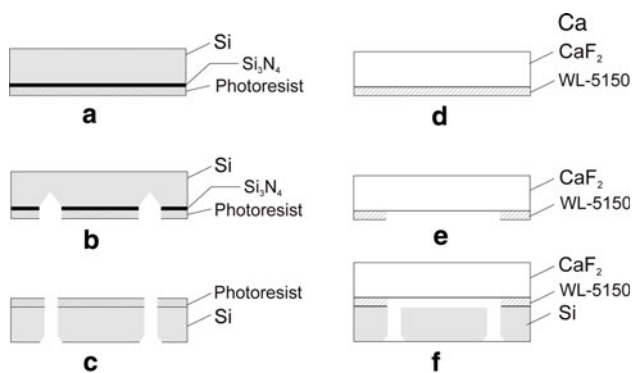
Fig. 6 *Top* fabrication procedure of the micromixer: **a** spin coating of positive photoresist on Si wafer, **b** KOH etching of the inlet holes after a photolithographic step and plasma etching of the Si_3N_4 layer, **c** spin coating of the other side and DRIE etching of the inlet channels, **d** spin coating of the CaF_2 wafer with a photopatternable silicone, **e** photo-patterning of the mixing channel, **f** bonding of the CaF_2 and the Si wafer. *Bottom* image of the custom built chip holder and a mounted micromixer, which enables using standard fittings as fluid connectors
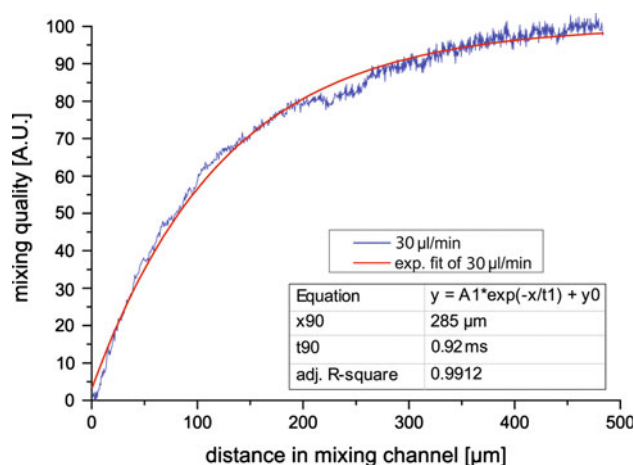

Fig. 7 Recorded measurement result with the optimized wedge shaped design. The mixing quality was averaged over the channel width. The mixing time was calculated with MATLAB after an exponential fit was applied. Measurements along the mixing channel (x-axis) correspond to a reaction time defined by the flow velocity

Fig. 8 Recorded measurement result with the straight shaped design. The mixing quality was averaged over the channel width. The mixing time was calculated with MATLAB after an exponential fit was applied. Measurements along the mixing channel (x-axis) correspond to a reaction time defined by the flow velocity
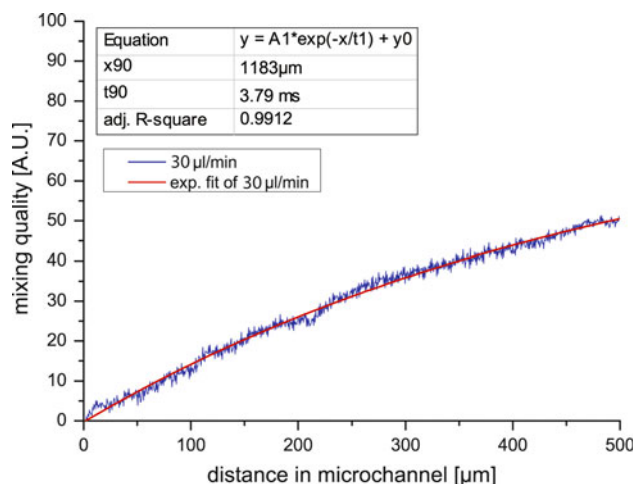
0.48 ms between two spectra. At each measurement spot 32 co-additions at a spectral resolution of 4 cm^{-1} were recorded. The diffusion coefficients of D_2O and H_2O are found in Crowell and Bartels (1996), which lead to calculated mixing times of about 1 ms as outlined in Sec. 2.1. D_2O was purchased from Sigma Aldrich (St. Louis, MO, USA) whereas deionized H_2O was taken from the lab. Each experiment consisted of two separate measurements. First, both syringes were filled with water and background measurements along the mixing channel were recorded. This procedure was necessary due to slight inhomogeneities in the transmission behavior along the mixing channel. Afterwards, one syringe was replaced with a syringe filled with D_2O and the experiment was repeated while mixing D_2O and H_2O. After both measurements were recorded, the absorbance spectrum was calculated with *OPUS* and plotted with *Origin*, Fig. 9. The dataset shows the deformation vibrations of H_2O (1640 cm^{-1}), HDO (1456 cm^{-1}) and

D_2O (1212 cm^{-1}), measured along the mixing channel. The H_2O band appears negative due to the fact that H_2O served as the background of the measurement (Fig. 9a). The integrated band area of the HDO and H_2O bands, including mono-exponential fits to the data, are presented in Fig. 9b.

3 Conclusion

The microfluidic device presented is the first highly uniform multilamination mixer utilizing wedge shaped inlet channels, which can be applied for very fast time resolved
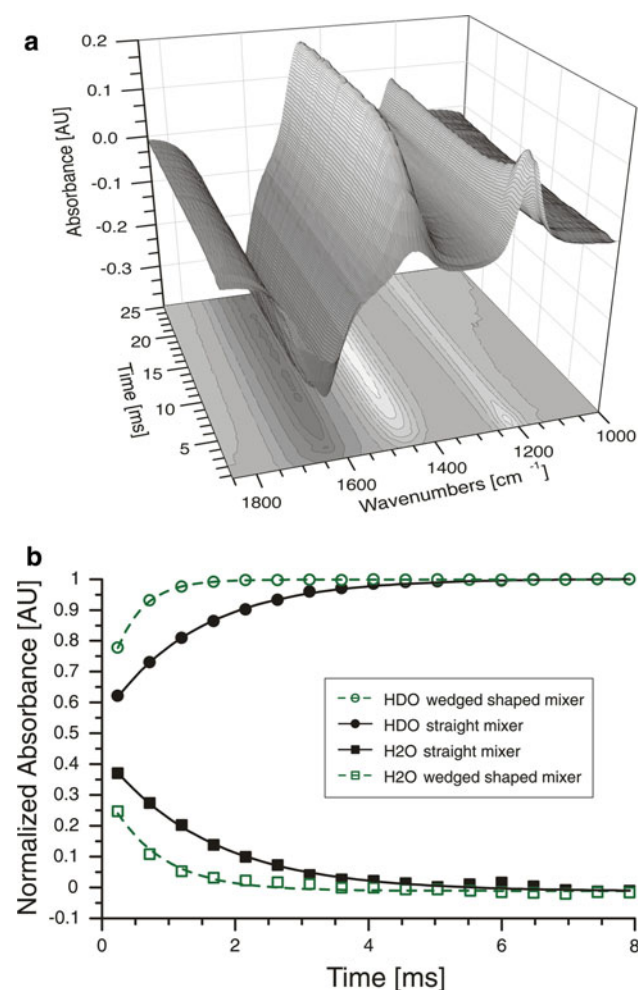
fluids are mixed and monitored before a third reagent is added (e.g., to quench the chemical reaction). The easy setup and handling with the custom holder and standard fluid connectors make this device an attractive tool for studying chemical reaction kinetics. In further experiments, this micromixer could also be used for determining diffusion coefficients of different fluids.

Fig. 9 a This dataset shows the deformation vibrations of H_2O (1640 cm^{-1}), HDO (1456 cm^{-1}) and D_2O (1212 cm^{-1}) measured along the mixing channel. The H_2O band appears negative due to the fact that H_2O served as the background for the measurement, **b** shows the integrated band area of the HDO and H_2O bands including monoexponential fits to the data, resulting in reaction time constants of H_2O 1.4 ms for the straight shaped mixer and 0.4 ms for the wedge shaped mixer

optical and infrared measurements. Simulated mixing times of around 1 ms could be confirmed through optical and infrared spectroscopic methods. Due to the optimized wedge shaped inlet channel, this design is applicable for very low flow rates down to 1 µl/min and hence reduces costly reagent consumption to a minimum. Further, this device is applicable for IR spectroscopy to analyze the so far unclear kinetics of chemical reactions. The fabrication procedure of this device is simple and time efficient as the channel structures are processed on a silicon wafer by standard micromachining techniques. An easy device upgrade for mixing more than two reagents is possible by simply adding further lamination layers. In the same way, a two stage mixer can be realized where first two reacting

References

Ahmed D, Mao X, Shi J, Juluri BK, Huang TJ (2009) A millisecond micromixer via single-bubble-based acoustic streaming. Lab Chip 9(18):2738–2741

Chan KLA, Gulati S, Edel JB, de Mello AJ, Kazarian SG (2009) Chemical imaging of microfluidic flows using atr-ftir spectroscopy. Lab Chip 9(20):2909–2913

Chen L, Wang G, Lim C, Seong GH, Choo J, Lee EK, Kang SH, Song JM (2009) Evaluation of passive mixing behaviors in a pillar obstruction poly(dimethylsiloxane) microfluidic mixer using fluorescence microscopy. Microfluid Nanofluid 7(2):267–273

Cortes-Quiroz CA, Zangeneh M, Goto A (2009) On multi-objective optimization of geometry of staggered herringbone micromixer. Microfluid Nanofluid 7(1):29–43

Crowell R, Bartels DM (1996) H2O/D2O Isotope effect in geminate recombination of hydrated electron. J Phys Chem 100:17713–17715

Gambin Y, Simonnet C, VanDelinder V, Deniz A, Groisman A (2010) Ultrafast microfluidic mixer with three-dimensional flow focusing for studies of biochemical kinetics. Lab Chip 272(23):5962–5970

Hardt S, Drese KS, Hessel V, Schnfeld F (2005) Passive micromixers for applications in the microreactor and TAS fields. Microfluidics Nanofluidics 1(2):108–118

Hinsmann P, Frank J, Svasek P, Harasek M, Lendl B (2001) Design, simulation and application of a new micromixing device for time resolved infrared spectroscopy of chemical reactions in solution. Lab Chip 1(1):16–21

Hinsmann P, Haberkorn M, Frank J, Svasek P, Harasek M, Lendl B (2001) Time-resolved FT-IR spectroscopy of chemical reactions in solution by fast diffusion-based mixing in a micromachined flow cell. Appl Spectrosc 55(3):241–251

Hossain S, Ansari MA, Kim KY (2009) Evaluation of the mixing performance of three passive micromixers. Chem Eng J 150(2–3):492–501

Johansson L, Johansson S, Nikolajeff F, Thorslund S (2009) Effective mixing of laminar flows at a density interface by an integrated ultrasonic transducer. Lab Chip 9(2):297–304

Jung SY, Liu Y, Collier CP (2008) Fast mixing and reaction initiation control of single-enzyme kinetics in confined volumes. Langmuir 24(9):4439–4442

Kanai M, Uchida D, Sugiura S, Sato H, Mori Y, Sakamoto K, Nakanishi H, Shoji S (2002) Optimal design of the micromixer using nonhomogeneous multilayer laminar flow. In: Proc. MicroTAS, vol 1, pp 73–75

Kauffmann E, Darnton N, Austin R, Batt C, Gerwert K (2001) Lifetimes of intermediates in the beta-sheet to alpha-helix transition of beta-lactoglobulin by using a diffusional ir mixer. Proc Natl Acad Sci USA 98(12):6646–6649

Lipman E, Schuler B, Bakajin O, Eaton W (2003) Single-molecule measurement of protein folding kinetics. Science 301(5637):1233–1235

Mansur EA, Ye M, Wang Y, Dai Y (2008) A state-of-the-art review of mixing in microfluidic mixers. Chinese J Chem Eng 16(4):503–516

Mao X, Juluri BK, Lapsley MI, Stratton ZS, Huang TJ (2010) Milliseconds microfluidic chaotic bubble mixer. Microfluid Nanofluid 8(1):139–144

Nguyen N, Wu Z (2005) Micromixers—a review. J Michromech Microeng 15(2):R1–R16

Nguyen NT, Wereley ST (2002) Fundamentals and Applications of Microfluidics. MEMS Series, Artech House

Park JM, Seo KD, Kwon TH (2010) A chaotic micromixer using obstruction-pairs. J Micromech Microeng 20(1):015023 (11 pp)

Rigler A, Wagner C, Svasek P, Jachimowicz A, Hudek P, Kraft M, Vellekoop M (2008) Improved lamination micromixer with wedge shaped inlet channels for IR spectroscopy. In: Proceedings of 22nd international eurosensors conference

Wen CY, Yeh CP, Tsai CH, Fu LM (2009) Rapid magnetic microfluidic mixer utilizing AC electromagnetic field. Electrophoresis 30(24, Sp. Iss. SI):4179–4186

Williams AM, Griffiths DJ, Vlachos PP (2009) Laminar mixing using oscillating cantilevered ionic polymer actuators. Sensor Acutat A Phys 153(1):105–113